Wind and Structures, Vol. 13, No. 6 (2010) 557-580
DOI: http://dx.doi.org/10.12989/was.2010.13.6.557

Large eddy simulation of wind effects on a super-tall building

Shenghong Huang[1,2] and Q.S. Li*[2]

[1]*School of Engineering Science, University of Science and Technology of China, Hefei, 230026, P.R. China*
[2]*Department of Building and Construction, City University of Hong Kong, Kowloon, Hong Kong*

(Received September 14, 2009, Accepted July 16, 2010)

Abstract. A new inflow turbulence generation method and a combined dynamic SGS model recently developed by the authors were applied to evaluate the wind effects on 508 m high Taipei 101 Tower. Unlike the majority of the past studies on large eddy simulation (LES) of wind effects on tall buildings, the present numerical simulations were conducted for the full-scale tall building with Reynolds number greater than 10^8. The inflow turbulent flow field was generated based on the new method called discretizing and synthesizing of random flow generation technique (DSRFG) with a prominent feature that the generated wind velocity fluctuations satisfy any target spectrum and target profiles of turbulence intensity and turbulence integral length scale. The new dynamic SGS model takes both advantages of one-equation SGS model and a dynamic production term without test-filtering operation, which is particular suitable to relative coarse grid situations and high Reynolds number flows. The results of comparative investigations with and without generation of inflow turbulence show that: (1) proper simulation of an inflow turbulent field is essential in accurate evaluation of dynamic wind loads on a tall building and the prescribed inflow turbulence characteristics can be adequately imposed on the inflow boundary by the DSRFG method; (2) the DSRFG can generate a large number of random vortex-like patterns in oncoming flow, leading to good agreements of both mean and dynamic forces with wind tunnel test results; (3) The dynamic mechanism of the adopted SGS model behaves adequately in the present LES and its integration with the DSRFG technique can provide satisfactory predictions of the wind effects on the super-tall building.

Keywords: large eddy simulation; subgrid scale model; inflow turbulence generation; computational fluid dynamics; tall building; wind effect; wind tunnel test; typhoon.

1. Introduction

With changing of earth environment, strong windstorms such as typhoons and hurricanes become more and more disastrous and frequently occur in recent years. Since most tall buildings have relatively low natural frequencies which may be coincident with some frequency bands of typhoons, tall buildings, especially super-tall buildings (building height > 400 m), located in typhoon-prone regions, may be susceptible to severe forces induced by typhoons. However, current codes and standards are actually not guaranteed to fully cover the design of super-tall buildings. Therefore,

* Corresponding Author, Associate Professor, E-mail: bcqsli@cityu.edu.hk

comprehensive studies of wind effects on super-tall buildings under strong typhoon conditions are of particular importance and necessity.

Currently, there are mainly three means to investigate the wind loads and effects on tall buildings: (1) wind tunnel testing; (2) field measurements of prototype structures; (3) numerical simulation. Wind tunnel testing is a relatively mature technology in wind engineering, which has been developed and widely used for more than three decades, and it has been a primary tool to determine cladding pressures and overall wind-induced loads on tall buildings. However, wind tunnel testing has several limitations, for instance, Reynolds number limitations, since most wind tunnel applications are generally conducted using scaled models (1/100~1/500) of tall buildings. In other words, it is difficult or even impossible to determine the wind loads on tall buildings in wind tunnel tests with the same Reynolds numbers as those in full-scale. Another limitation is that conventional wind tunnels cannot generate boundary layer wind flows with sufficient large values of turbulence integral length scales. Field measurements (Li *et al*. 1998, 2000, 2003, 2004, 2008) reveal that in the atmospheric boundary layer the longitudinal turbulence integral scale exhibited considerable variations from site to site. The variations were also significant for the measurements made in different typhoons at the same measurement site. The longitudinal turbulence integral scales were observed to vary between 30 m and 550 m at elevations of 330 m-400 m above the city centers of Hong Kong, Shenzhen and Shanghai during the passages of several typhoons. According to the field measurement results, it was estimated that the ratio of longitudinal turbulence integral scale to building characteristic length for typical super-tall buildings in the atmospheric boundary layer may be more than 10. However, this ratio simulated in wind tunnels is usually of the order of unity. As reported by Li and Melbourne (1995, 1999), longitudinal turbulence integral scale has a significant effect on the estimation of peak and fluctuating wind pressures on building models. Thus, it is clear that there is a source of uncertainty involved in wind tunnel modeling which needs to be further investigated.

It has been recognized that the most reliable evaluations of wind effects are obtained from measurements on prototype structures. Field measurements are able to provide the fundamental knowledge in wind loading and responses of tall buildings. A number of full-scale measurements of wind effects on tall buildings have been made throughout the world in recent years, including the extensive measurement program on four Chicago tall buildings currently being undertaken by Notre Dame University and the University of Western Ontario (Kijewski-Correa 2003) and on ten super-tall buildings in Hong Kong and Mainland China by City University of Hong Kong (Li *et al*. 1998, 2000, 2003, 2004, 2008). Although the obtained data sets are very important and valuable for further understanding of wind effects on super-tall buildings, the chance to conduct full-scale measurements is quite rare. Besides, because of site condition limitations, measuring points (e.g., cladding pressures) on a prototype tall building are usually much less than those in a wind tunnel test and consequently the information obtained from full-scale measurements is limited.

Different from wind tunnel testing and field measurements, numerical simulation which is based on solutions of theoretical or computational models is a convenient and cost-effective tool to determine wind effects on tall buildings, especially due to rapid development of computational methods and computer resource in recent years (Stathopoulos 1997, Baker 2007, Huang *et al*. 2007). Computational Fluid Dynamics (CFD) techniques, such as Large Eddy Simulation (LES), Reynolds Averaged Navier-Stokes Equations (RANS) Models, and so on, have been developed to predict wind loads on structures and wind flows around buildings (Zhang *et al*. 2006, Huang *et al*. 2007, Jiang *et al*. 2008, Huang and Li 2010, Li *et al*. 2010), while computational structural

dynamics (CSD) approaches, such as finite element method, nonlinear analysis techniques, and so on, were used to predict structural responses based on the computed wind loads.

One of the most attractive aspects of numerical simulation is that abundant information such as wind flow field, pressure distributions on building surfaces, overall wind-induced loads as well as structural responses (displacement, acceleration, strain, stress etc.) can be predicted by computers based on CFD and CSD. Furthermore, the drawbacks of wind tunnel testing, e.g., Reynolds number and turbulence integral length scale limitations mentioned previously, can be overcame if adequate strategies are adopted in numerical simulations. However, as discussed by Stathopoulos (1997), Murakami (1998) and Baker (2007) among others, limitations inevitably exist in computational wind engineering and one of the most key issues is high Reynolds number turbulence simulation for bluff-body flow. In fact, high Reynolds number turbulence simulation itself is one of the most difficult problems yet to be solved in turbulence research fields, although numerous models and numerical methods have been proposed continuously.

Wind around a building is a typical bluff-body flow, in which turbulence plays a vitally important role of generation of dynamic wind loads on the building and most turbulent flows encountered in wind engineering are associated with high Reynolds number due to large building dimensions and high wind speeds. Hence, CFD techniques should faithfully model the turbulence structures within the atmospheric boundary layer with high Reynolds number. Efforts for such practices using unsteady RANS techniques have been made with limited success (Rodi 1997, Huang *et al*. 2007), while LES (Nozu *et al*. 2008, Tamura 2008) or DES (detached eddy simulation) techniques present very encouraging results (Squires *et al*. 2008). However, most previous LES studies in wind engineering focused on numerical simulations for scaled building models for the sake of simplicity. With the development of computing resource and LES models in recent years, it is more appealing to conduct full-scale size simulations of wind effects for practical wind engineering applications. Recent representative works on this subject include a study conducted by Tamura (2008), in which full-scale wind flow fields in urban areas were simulated by LES. Their results revealed that LES is able to reproduce an overall flow field in an urban area and in particular, Nozu *et al*. (2008) reported that their full-scale LES predictions matched the measured pressure distributions on surfaces of a tall building qualitatively.

Tamura (2008) summarized that there are three key issues for practical use of LES in wind engineering: (1) Generation of inflow turbulence; (2) Sophisticated sub-grid scale (SGS) turbulence modeling; (3) Numerical discretization with conservation of various physical quantities for modeling complicated geometries.

A very important issue in obtaining accurate LES results is to generate a flow field as an inflow boundary condition (inflow turbulence) which satisfies prescribed spatial correlations and turbulence characteristics. The importance of inflow turbulence generation for wind engineering applications lies in the fact that natural wind is essentially a turbulent and unsteady flow with very high Reynolds numbers and hence, the oncoming flow in computational domain should have these inherent characteristics of natural wind. Besides, since high speed wind near the earth manifests very strong inhomogeneity and anisotropy, generation of inflow turbulence satisfying these characteristics of natural wind is a challenging task. Currently, there are two kinds of inflow turbulence generation methods. The first method is to numerically simulate turbulent flows in an auxiliary computational domain (often called a driver region where a fluid flow is driven) and the other method provides generation of inflow turbulence by artificial numerical models. In Nozawa and Tamura's (2005) study, the first kind of method was used, in which a roughness block

distribution was included in their simulation for deriving the inflow conditions. In a recent study of the authors, a general inflow turbulence generator for LES was presented (Huang *et al*. 2010), which belongs to the second kind of method and was developed based on discretizing and synthesizing of random flow generation (DSRFG) technique. The newly developed method was proved to be able to generate a fluctuating turbulent flow field satisfying desired spectra and spatial correlations including inhomogeneity and anisotropy (Huang *et al*. 2010). In addition, the DSRFG method has built-in divergence-free mechanism in random velocity generation, thus no velocity correction and preliminary storage for time-sequential data are needed.

The second important issue is sophisticated SGS turbulence modeling. Up to now, the development of SGS models for LES has experienced three stages since the primitive work of Smagorinsky (1963), namely, the algebraic eddy viscosity models (Germano *et al*. 1991, Lilly 1992, Zang 1993, Vreman *et al*. 1994, Ghosal *et al*. 1995, Nicoud and Ducros 1999), one-equation eddy viscosity models (Yoshizawa and Horiuti 1985, Kim and Menon 1995, 1999, Krajnovic and Davidson 2002, Kajishima and Nomachi 2006) and two-equation eddy viscosity models (Gallerano *et al*. 2005). The aim of such developments is to accurately model the SGS and the energy transfer mechanism with GS (grid-scale) for high Reynolds number flows. However, in review of the majority of the existing SGS models, it is found that there are two contradictions limiting their applications in engineering practice. The first is the contradiction of low-order discretization and unstructured grid (necessarily adopted for complex engineering problems) with the test-filtering operation that has been used in most dynamic SGS models. The second is the contradiction of non-equilibrium characteristic (in high Reynolds number flows and coarse grid situations) with local equilibrium assumption involved in algebraic SGS models, despite some models such as the wall-adapting local eddy viscosity model (WALE) model (Nicoud and Ducros 1999) are actually very simple, robust and suitable for engineering applications. So, it may be necessary and significant to develop a SGS model that is engineering-oriented and is capable of solving some practical engineering problems effectively. Recently, we developed a new dynamic one-equation subgrid-scale (SGS) model for LES (Huang and Li 2010) which has the advantages of both the dynamic one-equation SGS model (Kajishima and Nomachi 2006) and the WALE model (Nicoud and Ducros 1999). The prominent features of this SGS model are: (1) one-equation model, suitable for relative coarse grid situations and simulation of high Reynolds number flows; (2) no test-filtering operation is needed in determination of dynamic parameters, suitable for relative low-order numerical discritization and unstructured or hybrid grid situations; (3) treating the production of SGS kinetic energy and energy loss in grid-scale (GS) portion due to SGS motion with different dynamic mechanisms, which is considered to be more reasonable than the local and instantaneous dynamic mechanism adopted by most existing one-equation dynamic SGS models.

In this paper, both the inflow turbulence generator and the SGS model newly developed by the authors are applied to evaluate the wind effects on Taipei 101 Tower. As shown in Fig. 1, Taipei 101 Tower is a 101-floor and 508 m high landmark skyscraper located in Xinyi District of Taipei, Taiwan. The primary objective of the present investigation is to evaluate the wind effects on the super-tall building through full-scale size LES based on our new models and techniques which have been validated for wind engineering applications with Reynolds number less than 10^5 (Huang and Li 2010, Huang *et al*. 2010). The accuracy and effectiveness of the proposed models for LES of wind effects on the full-scale super-tall building with Reynolds number greater than 10^8 will be examined and discussed in detail.

Fig. 1 Photo of Taipei 101 Tower

2. Methodology

2.1 Governing equations of LES

The governing equations of LES for incompressible flow are obtained by conducting the grid filtering operation to the Navier-Stokes (NS) equation and continuity equation. The filtered continuity equation and the NS equation are expressed as

$$\frac{\partial \bar{u}_i}{\partial x_i} = 0 \tag{1}$$

$$\frac{\partial \rho \bar{u}_i}{\partial t} + \frac{\partial (\rho \bar{u}_i \bar{u}_j)}{\partial x_j} = -\frac{\partial}{\partial x_i}\left(\bar{p} + \frac{2}{3}\rho k_{sgs}\right) + \frac{\partial}{\partial x_j}[2\rho(\upsilon_s + \upsilon)\bar{S}_{ij}] \tag{2}$$

where $\bar{u}_i$ denotes the GS component of velocity, $\bar{p}$ represents the GS component of pressure, ρ denotes the fluid density, υ is the kinetic viscosity of fluid, υ_s is the SGS eddy viscosity, given by

$$\upsilon_s = C_v \Delta_v \sqrt{k_{sgs}} \tag{3}$$

Here C_v is regarded as a constant instead of a dynamical parameter, as suggested by Kajishima and Nomachi (2006). Δ_v is the characteristic length, and k_{sgs} is the SGS kinetic energy. According to Okamoto and Shima (1999), Δ_v is calculated by

$$\Delta_v = \frac{\bar{\Delta}}{1 + C_k \dfrac{\bar{\Delta}^2 \bar{S}^2}{k_{sgs}}} \tag{4}$$

The above equation is used here to meet the correct asymptotic behavior to a wall, in which C_k is a model constant, $\bar{S} = \sqrt{2\bar{S}_{ij}\bar{S}_{ij}}$. Since both C_v and Δ_v are non-negative values, υ_s cannot take a negative value, thus computation of Eq. (2) is expected to be numerically stable.

k_{sgs} is obtained from a transportation equation below

$$\frac{\partial k_{sgs}}{\partial t} + \frac{\partial \bar{u}_j k_{sgs}}{\partial x_j} = -\tau_{ij}\bar{S}_{ij} - C_\varepsilon \frac{k_{sgs}^{3/2}}{\bar{\Delta}} + \frac{\partial}{\partial x_j}\left[(C_d \Delta_v \sqrt{k_{sgs}} + \upsilon)\frac{\partial k_{sgs}}{\partial x_j}\right] - \varepsilon_w \tag{5}$$

In fact, Eq (5) is basically the same as the dynamic one-equation SGS model (OD model) proposed by Kajishima and Nomachi (2006) which suggested that the production term, i.e., $-\tau_{ij}\bar{S}_{ij}$, in the k_{sgs} equation, corresponding to the energy transfer from GS to SGS portion of turbulence kinetic energy, is *locally and instantaneously*, and thus is determined through dynamic procedure. Meanwhile, SGS stress in the filtered equation of motion, i.e., υ_s, is not identical locally and instantaneously, and thus is approximated by the eddy viscosity model given indirectly by k_{sgs}.

In implementation of Kajishima and Nomachi's model, the dynamic procedure of the dynamic Smagorinsky model (DSM) proposed by Germano *et al*. (1991) is used to construct the production term $-\tau_{ij}\bar{S}_{ij}$, in which the test-filtering procedure has to be used to determine the coefficient dynamically. Different from this method, Huang and Li (2010) suggested that the production term $-\tau_{ij}\bar{S}_{ij}$ in Eq. (5) is constructed by

$$-\tau_{ij}\bar{S}_{ij} = \left((C_W^*\bar{\Delta})^2 \frac{(S_{ij}^d S_{ij}^d)^{\frac{3}{2}}}{(\bar{S}_{ij}\bar{S}_{ij})^{\frac{5}{2}} + (S_{ij}^d S_{ij}^d)^{\frac{5}{4}}} \right) |\bar{S}|^2 - \frac{2}{3} k_{sgs}\delta_{ij}\bar{S}_{ij} \tag{6}$$

where

$$S_{ij}^d = \frac{1}{2}(\bar{g}_{ij}^2 + \bar{g}_{ji}^2) - \frac{1}{3}\delta_{ij}\bar{g}_{kk}^2 \tag{7}$$

$$\bar{g}_{ij} = \frac{\partial \bar{u}_i}{\partial x_j} \tag{8}$$

$$C_W^* = \begin{cases} C_W \dfrac{|\bar{\Omega}|}{|\bar{S}|} & when \ \dfrac{|\bar{\Omega}|}{|\bar{S}|} < 1 \\ C_W & when \ \dfrac{|\bar{\Omega}|}{|\bar{S}|} \geq 1 \end{cases} \tag{9}$$

There are several advantages related to this formulation:

1) All the turbulence structures related to kinetic energy dissipation can be detected by $S_{ij}^d S_{ij}^d$ without the test filtering operation.
2) $S_{ij}^d S_{ij}^d$ behaves like y^2 near wall, which guarantees the production term going naturally to zero (y^3) in the vicinity of a wall so that neither (dynamic) constant adjustment nor damping function is needed to compute wall bounded flows.
3) $S_{ij}^d S_{ij}^d = 0$ in case of pure shear flow, produces zero production of k_{sgs}. Thus, it is possible to reproduce the laminar to turbulent transition process through the growth of linear unstable modes.

It is worthy noting that using the velocity gradient tensor $\bar{g}_{ij} = \dfrac{\partial \bar{u}_i}{\partial x_j}$ to construct the operator S_{ij}^d for

calculating SGS viscosity dynamically was firstly introduced by Nicoud and Ducros (1999) in their WALE model. In our newly developed SGS model, the dynamic mechanism of the WALE model was introduced into the OD model by Eq. (6), which combines both advantages of the OD model and the WALE model.

2.2 Inflow turbulence generator

In wind engineering, most measured turbulence spectra of wind speed fluctuation were found to obey the von Karman model (Li *et al*. 2004, 2005). Therefore, generation of an inflow turbulent flow field satisfying a target spectrum following the von Karman model is of great significance for accurate evaluation of wind effects on building and structures by LES. In the present investigation, a newly developed inflow turbulence generation method, namely DSRFG, proposed by the authors (Huang *et al*. 2010), is adopted to produce a fluctuating velocity field satisfying the von Karman spectrum. The detailed derivation of the DSRFG method is given by Huang *et al.* (2010), and a brief formulation of the method is presented below

$$\mathbf{u}(\mathbf{x}, t) = \sum_{m=k_0}^{k_{\max}} \mathbf{u}_m(\mathbf{x}, t) = \sum_{m=k_0}^{k_{\max}} \sum_{n=1}^{N} [\mathbf{p}^{m,n} \cos(\tilde{\mathbf{k}}^{m,n} \cdot \tilde{\mathbf{x}} + \omega_{m,n} t) + \mathbf{q}^{m,n} sin(\tilde{\mathbf{k}}^{m,n} \cdot \tilde{\mathbf{x}} + \omega_{m,n} t)] \quad (10)$$

where $\mathbf{p}^{m,n} = \frac{\varsigma \times \mathbf{k}^{m,n}}{\left|\varsigma \times \mathbf{k}^{m,n}\right|} \sqrt{a \frac{4E(k_m)}{N}}$, $\mathbf{q}^{m,n} = \frac{\xi \times \mathbf{k}^{m,n}}{\left|\xi \times \mathbf{k}^{m,n}\right|} \sqrt{(1-a) \frac{4E(k_m)}{N}}$, $\tilde{\mathbf{x}} = \frac{\mathbf{x}}{L_s}$, $\tilde{\mathbf{k}}^{m,n} = \frac{\mathbf{k}^{m,n}}{k_0}$, $\left|\mathbf{k}^{m,n}\right| = k_m$, $\omega_{m,n} \in N(0, 2\pi k_m)$, ς and ξ are vector form of ς_i^n and ξ_i^n, respectively, and $\varsigma_i^n, \xi_i^n \in N(0, 1)$. k_m is wave number. L_s is turbulence integral length scale which is an important parameter used as the scaling factor for spatial correlation. a is a random number uniformly distributed between 0~1. N = 100~200 (sampling number for each wave number k_m) are found to be accurate enough and economical for most applications in wind engineering.

It is worthy noting that: the velocities generated by LES are those resolved by LES filter (grid) while velocities simulated by the DSRFG are instantaneous velocities. In fact, the instantaneous velocities are applied to inlet boundary only, which will be then filtered by grid in computation domain and be transformed into velocities and SGS viscosities resolved by grid through SGS model. Therefore, if the grid scale between the target building and the inlet are fine enough, most parts of velocity fluctuations generated by the DSRFG at the inlet can be resolved and acted on the building as dynamic loads.

2.3 Implementing and numerical setup in FLUENT

The CFD code used in the present research is commercial software FLUENT. The models proposed and developed by the authors (Huang and Li 2010, Huang *et al*. 2010) were implemented as a User Defined Function (UDF) library, which was integrated into the FLUENT code by programming technique of user defined scalar and function hooks (Fluent Inc. 2003).

The numerical setup includes:

(1) The solver for incompressible flow in FLUENT employs an algorithm which belongs to a general class of methods called the projection method (Chorin 1968). In the projection

method, the governing equations are solved sequentially. Because the governing equations are non-linear and coupled, the pressure velocity coupling method must be carried out iteratively in order to obtain a converged numerical solution, wherein the constraint of mass conservation (continuity) of the velocity field is achieved by solving a pressure (or pressure correction) equation. The pressure equation is derived from the continuity and the momentum equations in such a way that the velocity field, corrected by the pressure, satisfies the continuity.

(2) The pressure velocity coupling method chosen for the present simulation is SIMPLC (Semi-Implicit Method for Pressure-Linked Equations Consistent) algorithm (Van Doormaal and Raithby 1984), which is one of variants of the basic SIMPLE algorithm and is characterized by convergence acceleration with modification to face flux correction equation. For meshes with some degree of skewness, a process called 'skewness correction' is introduced to reduce convergence difficulties associated with highly distorted meshes, which includes initial solution of the pressure-correction equation, the recalculation of pressure-correction gradient and the update of the mass flux corrections (Ferziger and Peric 1996).

(3) The bounded central difference, a default convection scheme for LES in FLUENT, is used to discretize the convective terms of momentum equations for its relative low diffusivity. This kind of scheme is essentially based on the normalized variable diagram (NVD) approach (Leonard 1991) together with convection boundedness criterion (CBC). The bounded central differencing scheme is a composite NVD-scheme that consists of a pure central differencing, a blended scheme of the central differencing and the second-order upwind scheme, and the first-order upwind scheme. It should be noted that the first-order scheme is used only when the CBC is violated. The central differencing is also applied to discretize the diffusion term.

(4) The time derivative is discretized using the second order backward differences and the spatial discretization is treated implicitly. The non-linear terms produced by fully-implicit discretization of the convection term is solved by an iterative process.

Detailed validations of the new SGS model and numerical schemes of solver for wind engineering problems with Reynolds number in the range of 3000-70000 were presented in Huang and Li (2010), in which the accuracy of the adopted solver and the effectiveness of the proposed SGS model for simulations of wind flows around tall buildings were proved. In the present investigation, the same algorithms are adopted for simulations of wind effects on full-scale size Taipei 101 Tower, in which Reynolds number is greater than 10^8 .

2.4 Computational domain, mesh arrangement and boundary conditions

The computational model considered in this study includes a full-scale rigid model of Taipei 101 Tower. Computational domain, coordinate definition for this computational study are given in Fig. 2. As shown in Fig. 2, the computational domain covers $33D_b$ (D_b is the width of the building base, which is 62.4 m) in streamwise (X) direction ($-9.5<x/D_b<23.5$), 17 D_b in lateral or normal (Y) direction ($-8.5 < y/D_b < 8.5$) and 2 H in vertical (Z) direction. Such an arrangement ensures the blockage ratio of this building in the computational domain is less than 5%.

Fig. 3 shows the mesh arrangement for the computational domain involved the full-scale size Taipei 101 Tower. The primary characteristic of this mesh style is that the building is nested in a rectangular cylinder about two time lager than itself. For zones in the nesting rectangular cylinder, unstructured meshes are generated while for zones outside the nesting rectangular cylinder, structured meshes are applied. This arrangement makes it easy to generate meshes fine enough in

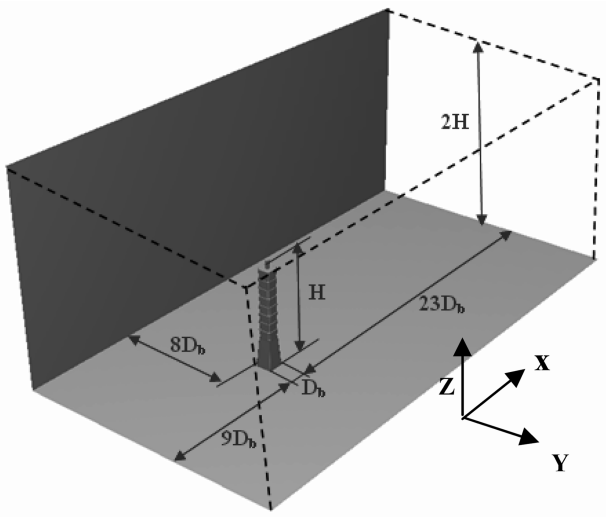

Fig. 2 Computational domain and boundary conditions

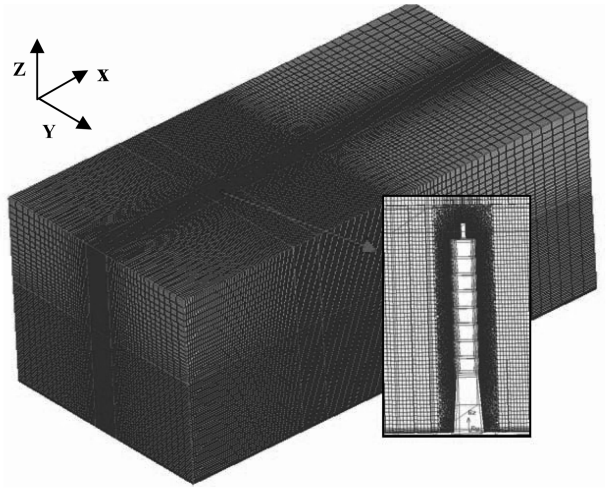

Fig. 3 Computational mesh arrangement

the neighborhood of the building surfaces while keeping the meshes in zones far away from the building surfaces unchanged or in a proper coarser state. Totally, about 5.5×10^6 cells are generated, and the meshes' grid stretching ratio in wake region is restricted to be less than 1.05 for reducing the difference of cut-off wave number between neighboring grids in the LES.

The boundary condition is set as follows: The inlet mean wind speed profile in the boundary layer of atmosphere is assumed to follow a power law

$$\frac{U}{U_{10}} = \left(\frac{Z}{Z_{10}}\right)^a \tag{11}$$

where U_{10} is the wind speed at the height of 10 m, a is the exponent of the mean wind speed

profile, Z is the height above ground surface. According to the statistical wind climate model and the typhoon simulations based on local wind speed measurements taken at Taipei Sungshan Airport, a 10-miniute mean wind speed of 43.27 m/s at 10 m height above ground and $a = 0.15$ are used in the present investigation (RWDI 1999), which are consistent with the design wind speed with 50 years return period as stipulated in the Taiwan Building Code.

Currently there is no sufficient field measurement information on variations of turbulence parameters from ground to height of 600 m, especially under high-wind conditions such as strong typhoons. Shiau (2000) conducted field measurements of strong wind (typhoon) at 26 m height on an observation tower located in Keelung harbor, about 20 km north of Taipei. The measured data show that the longitudinal turbulence intensity changes in the range from 0.18 to 0.23 and the longitudinal turbulence integral length scale varies from 40 m to 200 m in the wind speed range from 27 m/s to 45 m/s. Li *et al.* (2005) made field measurements on Central Plaza Tower (374 m) in Hong Kong and Di Wang Tower (384 m) in Shenzhen during a typhoon. Their measured turbulence intensity ranges from 0.02 to 0.4 and the integral length scale changes from 171 m to 600 m in the wind speed range from 2 m/s to 25 m/s. Based on these field data, the inflow turbulence profiles for turbulence intensity and integral length scale are determined, as shown in Fig. 4.

Non-slip wall boundary condition is set for the ground surface and the building surfaces, in which zero velocity on boundary surfaces is assumed. For the present LES, the SGS model guarantees the production term going naturally to zero (y^3) in the vicinity of a wall so the k_{sgs} on a wall is also set as zero.

For the outlet surface of the computation domain, a zero diffusion flux for all flow variables in the direction normal to the exit plane with an overall mass balance correction is set, since the distance of 23.5 D_b downstream of the building is enough to be fully-developed for wake flow.

For the side faces and upper boundary of the computational domain, free-slip boundary condition

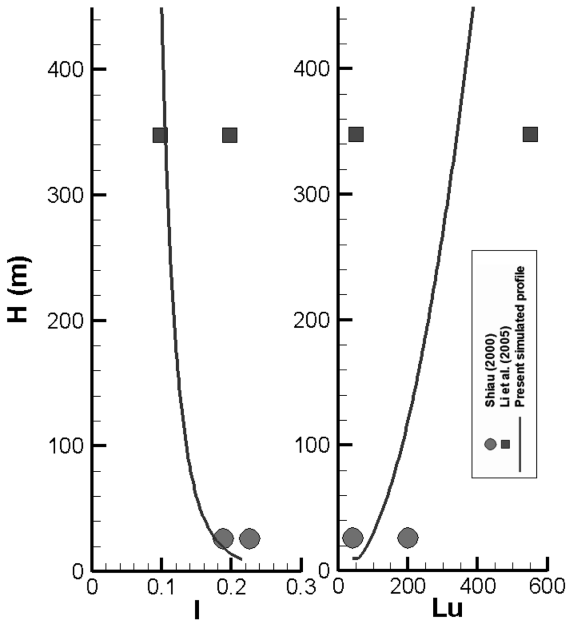

Fig. 4 Inflow turbulence profiles

is set, in which the normal velocity components and the normal gradients of all velocity components are set to be zero.

3. Results and discussions

The computations were performed on a high-performance cluster with 32CPUs. In consideration of the accuracy of the LES and computational expense, 0.05 seconds per time step was adopted for the present computation. Totally two cases were computed. The first case, hereinafter named CASE1, is corresponding to a smooth inflow condition, i.e., no turbulent velocity fluctuation was imposed at the inlet boundary. The second case, hereinafter called CASE2, is associated with a turbulent inflow field, in which the prescribed turbulence profiles shown in Fig. 4 were imposed through the proposed inflow turbulence generator described in Section 2.2. The purpose of such arrangements is to investigate the inflow turbulence effects on the wind loads on the super-tall building, Taipei 101 Tower.

First, 4000 time steps were iterated to obtain the results for CASE1, which is corresponding to 200 seconds physical time. The statistical averaging of flow field was taken for the last 2000 steps (100 seconds physical time). For CASE2, 16000 time steps were taken to obtain the results of the turbulent flow field. The statistical averaging of flow field was taken for the last 8000 steps (400 seconds physical time), which is about 12 times of the mean flow residence time in the solution domain.

The computational expense for the present LES is summarized here: memory usage 12GB, CPU time 733 hours with each time step about 60 seconds (5 sub iterations).

3.1 Comparison with wind tunnel test data

First, the along-wind force F_D, across-wind force F_L and tortional moment M were obtained based on the LES results. Table 1 lists their mean, peak and rms values. The counterpart results of the wind tunnel testing obtained by Rowan Williams Davies & Irwin Inc (RWDI) (1999) are also presented in Table 1 for comparison purposes. According to the results in Table 1, it is apparent that:

Table 1 Comparison with wind tunnel test data

	$\overline{F}_D$	$F_{D,\min}$ $F_{D,\max}$ σ_{F_D}	$\overline{F}_L$	$F_{L,\min}$ $F_{L,\max}$ σ_{F_L}	$\overline{M}$	$M_{\min}$ $M_{\max}$ σ_M
Units		$\times 10^7 N$				$\times 10^8 N\cdot m$
CASE1	6.7	6.46 7.1 0.13	0.005	-1 0.7 0.348	-0.02	-0.3 0.33 0.1
CASE2	7.1	4.0 9.3 0.6	0.04	-4.7 4.7 1.49	0.002	-2.5 2.0 0.7
RWDI (1999)	6.8	3.5 10 0.88 *	-0.6	-8.6 7.4 2.28 *	0.1	-3.9 4.1 1.14 *

* estimated by: (Maximum – Mean)/g, where g = 3.5 is peak factor

(1) For the mean force values, both the numerical results of CASE1 and CASE2 agree with the wind tunnel test data generally well. Specifically, CASE1 provides a computational value of $\overline{F}_D$ a little smaller than that of the model test while CASE2 slightly over-predicts it. For $\overline{F}_L$ and $\overline{M}$, the numerical results for the two cases are closed to zero; but the wind tunnel test results are -0.6 and 0.1, respectively. Such differences can be attributed to that the wind tunnel testing included all the main surrounding buildings around Taipei 101 Tower, while only the isolated building was considered in the numerical simulations. The interference effects considered in the model testing may cause the values of $\overline{F}_L$ and $\overline{M}$ to be different from zero.
(2) For the peak and rms values, the results obtained from CASE2 are in reasonable agreement with the wind tunnel test results, though the computed values are still generally smaller than their experimental counterparts. Compared with those from CASE2, the results from CASE1 are significantly smaller than the measured results, indicating that the inflow turbulence plays an important role in evaluation of the dynamic wind loads on the super-tall building and thus it is necessary to properly simulate the inflow turbulence in LES.
(3) As is well known, with the increase of building height, the across-wind dynamic force may exceed the along-wind dynamic force and becomes dominate dynamic loads on tall buildings, especially for a super-tall building such as Taipei 101 Tower. According to Table 1, $\sigma_{F_L} > \sigma_{F_D}$ are observed for CASE2 and from the wind tunnel test data, illustrating the correctness of the simulated results.

3.2 Flow field investigation

The flow pattern around a surface-mounted bluff body has been well investigated in the past (Martinuzzi 1992). The features of a typical flow field are summarized as: (1) A large separation region like a bubble developed around a bluff body; (2) unsteady vortex shedding and vortex interaction in wake region; (3) strong base suction inducing the contracted recirculating region when a bluff body stands in an atmospheric boundary layer (Davies *et al*. 1980). The instantaneous and mean velocity contours predicted by the present numerical simulation are shown in Figs. 7 and 8, respectively. It can be observed that the features of a typical flow field addressed above such as separation region and vortex shedding were correctly predicted by the present simulation, in particular:

(1) The mean separation region behind the building predicted by CASE2 (Fig. 8(b)) is obviously much more contracted than that of CASE1 (Fig. 8(a)). This is in accordance with the vortex shedding patterns shown in Figs. 7(a) and 7(b), in which CASE2 apparently predicts an earlier occurrence position of vortex shedding and stronger shedding intensity in the lateral separation boundary layer originated from the front surface corner.
(2) In Fig. 7(b), a large number of random vortex-like patterns present in the upstream region of the building, which is significantly different from the smooth flow pattern as shown in Fig. 7(a). These random vortex-like patterns were generated by the inflow turbulence generator (DSRFG) proposed by the authors (Huang *et al.* 2010). The generated inflow flow field satisfied the target profiles of turbulent intensity and turbulence length scale as shown in Figs. 5 and 6 as well as the target spectrum (von-Karman spectrum). These velocity fluctuations with different frequencies were coupled with vortex shedding modes in the lateral separation boundary layer, and thus intensive vortex shedding patterns were observed as shown in Fig. 7(b), which is an important generation mechanism of the dynamic wind forces on the tall

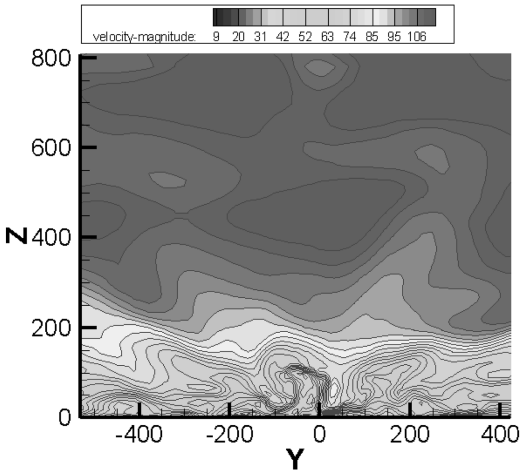

Fig. 5 Inflow velocity pattern generated by DSRFG

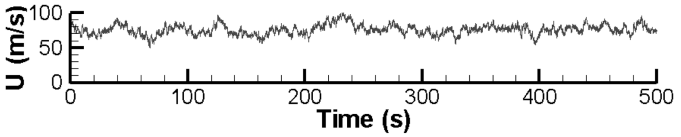

(a) u velocity sequence

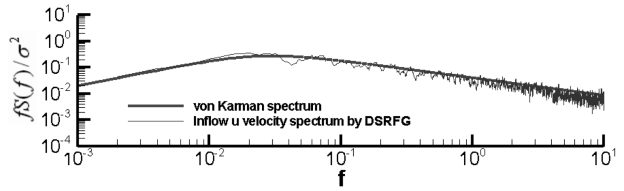

(b) spectrum of u velocity

Fig. 6 Velocity sequence and spectrum generated by DSRFG (I = 0.1, Lu = 372 m, Uavg = 75.7 m/s)

building, especially for the across-wind force F_L and tortional moment M.

(3) Intense vortex shedding also enhances the contraction of separation region and base suction as contrastively shown in Figs. 8(a) and 8(b), which induce a little increase of $\overline{F}_D$ for CASE2 as compared with that for CASE1 as listed in Table 1.

Both rms velocity contours of CASE1 and CASE2 are shown in Figs. 9(a) and 9(b), respectively. The statistical values represent the resolved velocity fluctuations of the solution domain. It is observed that the zones with large rms velocity magnitudes are mainly located in the separation and wake regions where vortex shedding is developed. For CASE1, as shown in Fig. 9(a), zero rms velocity magnitude is observed in the upstream of the building, which is in accordance with the smooth inflow boundary condition, and the rms velocity increases gradually from the lateral separation boundary layer to the edge of the separation bubble, where the vortex shedding from the two lateral separation boundary layers interacts. For CASE2, the oncoming rms velocity magnitude is non-zero, which represents existence of the inflow turbulence intensity. As expected, higher rms

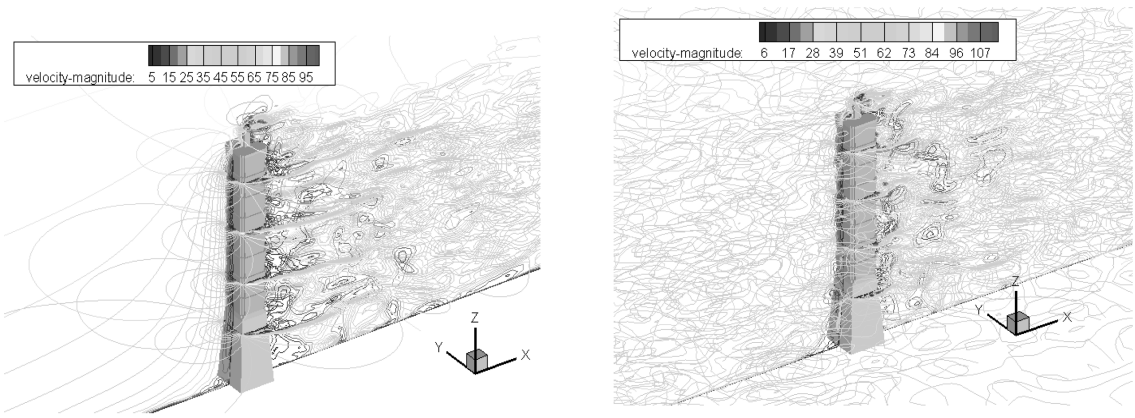

(a) CASE1 (b) CASE2

Fig. 7 Instantaneous velocity contours on Y = 0 m, Z = 92.4 m, Z = 176.4 m, Z = 260.4 m, Z = 344.4 m and Z = 419.4 m plane

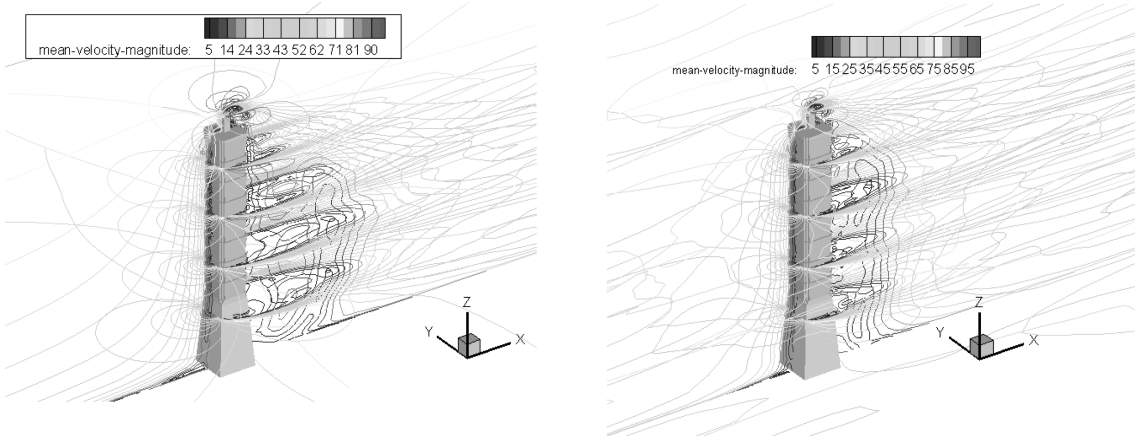

(a) CASE1 (b) CASE2

Fig. 8 Mean velocity contours on Y = 0 m, Z = 92.4 m, Z = 176.4 m, Z = 260.4 m, Z = 344.4 m and Z = 419.4 m plane

velocity magnitude is observed in Fig. 9(b), and the regions with high rms velocity magnitudes are closer to the side and back surfaces of the building than those in CASE1, indicating the existence of more intensive vortex shedding and turbulence intensity in CASE2.

The instantaneous SGS viscosity ratio (The ratio of the subgrid turbulence viscosity of the fluid to the laminar viscosity) contours predicted for CASE1 and CASE2 are shown in Figs. 10(a) and 10(b), respectively. The SGS viscosity represents the unresolved SGS scale energy of the solution domain. For CASE1, as shown in Fig. 10(a), zero SGS viscosity ratio is observed in the upstream of the building except in regions near the wall boundaries, which is reasonable as discussed in section 2.1, since the oncoming flow in the regions with zero SGS viscosity ratio is smooth and thus no k_{sgs} is detected. In regions of the lateral separation boundary layer, recirculation and vortex

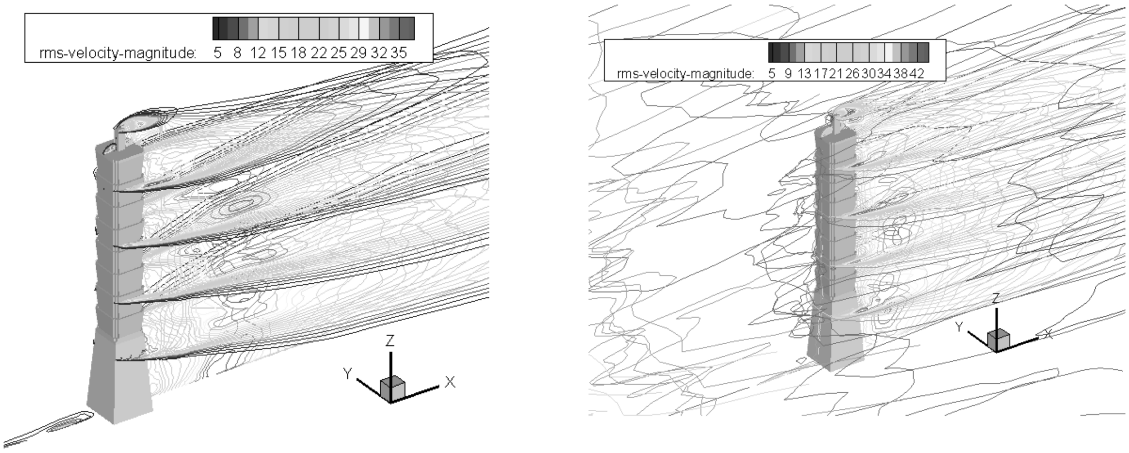

(a) CASE1 (b) CASE2

Fig. 9 rms velocity contours on Y = 0 m, Z = 92.4 m, Z = 176.4 m, Z = 260.4 m, Z = 344.4 m and Z = 419.4 m plane

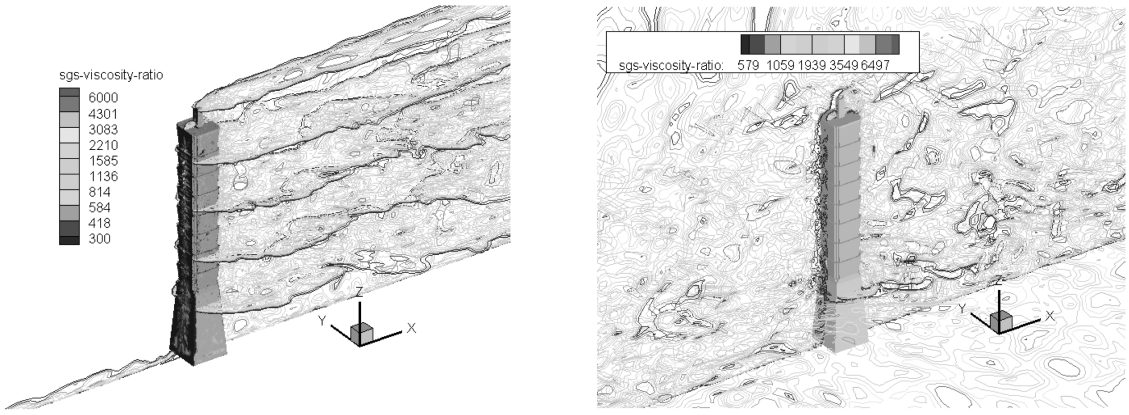

(a) CASE1
(Y=0 m, Z=92.4 m, Z=176.4 m, Z=260.4 m, Z=344.4 m and Z=419.4 m plane)

(b) CASE2
(Y=0 m, Z=92.4 m plane)

Fig. 10 SGS viscosity contours

shedding, the SGS viscosity ratio increases to the range of 500-6000 and a random pattern of the SGS viscosity ratio distribution is observed, this is a reasonable scene in consideration of the dynamic production term as previously discussed in section 2.1. For CASE2, as shown in Fig. 10(b), with the inflow turbulence imposed, the SGS viscosity ratio in the upstream region reasonably becomes a non-zero pattern, and the random distribution of SGS viscosity also indicates the correct mechanism of the dynamic SGS production.

3.3 Wind loading spectra

Fig. 11 shows comparison of time-histories of the total forces F_D, F_L, M obtained from the two

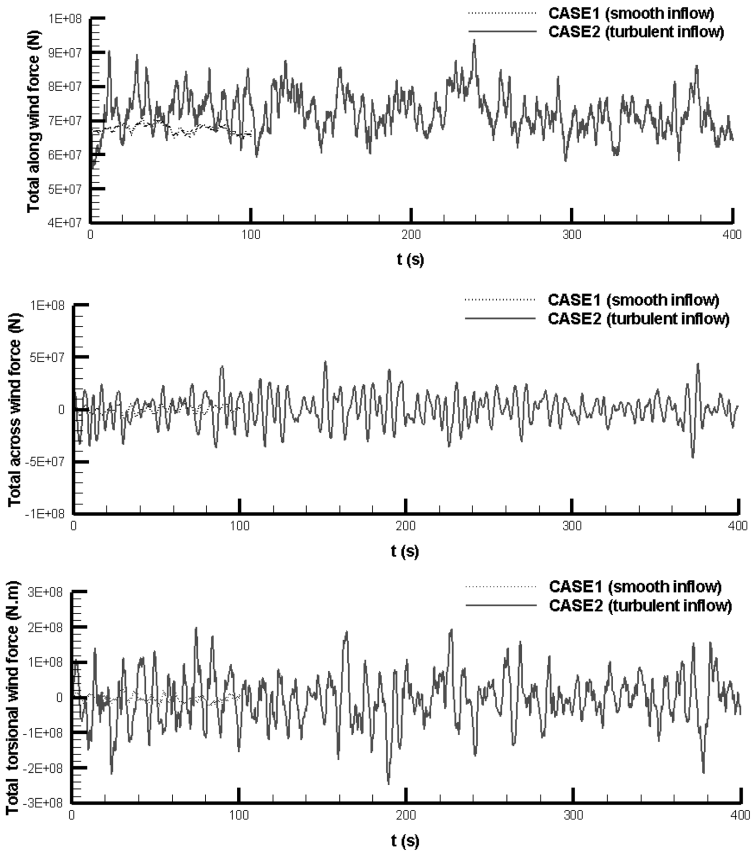

Fig. 11 Time histories of the total force F_D, F_L, M

cases. It can be observed that:

(1) CASE1 predicts relatively smooth wind-induced force fluctuations of F_D, F_L, M, while CASE2 yields several times larger values of the force fluctuations than those of CASE1 as shown in Figs. 11(a)-11(c). This should be attributed to the inflow turbulence fluctuations generated in CASE2.

(2) It is noted that the fluctuation patterns of the forces predicted by both CASE1 and CASE2 are irregular, especially for CASE2, which indicates that a large number of random vortex movements are predicted by the present SGS model.

Figs. 12 and 13 show comparison of the normalized power spectral density functions of the total forces and torsional moment F_D, F_L, M and the local F_D, F_L, M at five different heights where are H1 = 84 m ~ 92.4 m, H2 = 168 m ~ 176.4 m, H3 = 252 m~260.4 m, H4 = 336 m~344.4 m, H5 = 413 m ~ 419.4 m, respectively. H1 to H4 are located on the main building while H5 is located on the tower atop the main building and its width is only about 1/5 width of the main building. Table 2 lists the input mean wind speed and turbulence integral length scales at these locations. The target spectrum of the inflow wind velocity (von Karman spectrum) and the velocity spectra generated by DSRFG at the corresponding heights in the inlet boundary are also plotted in the figures. Based on those presented in these figures, it is observed that:

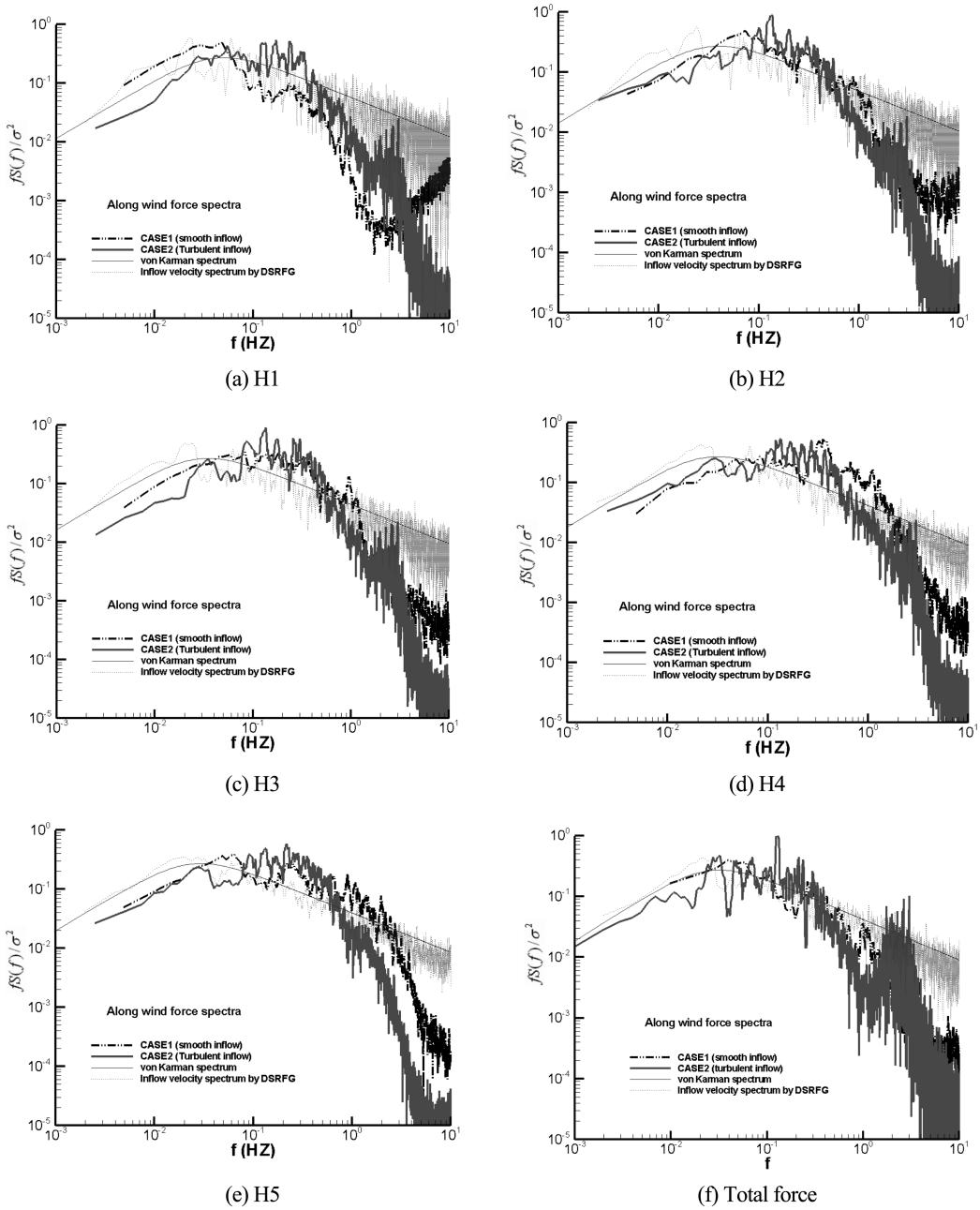

Fig. 12 Along-wind force spectra

(1) For the along-wind force F_D, the spectra predicted from the two cases are generally similar, as shown in Figs. 12(a)-12(f). However, some discrepancies are also presented. In Fig. 12(a), the power spectral magnitude for CASE2 in frequency range about 0.05~0.4 Hz increases obviously. Compared with the von Karman spectrum and that produced by the DSRFG, this

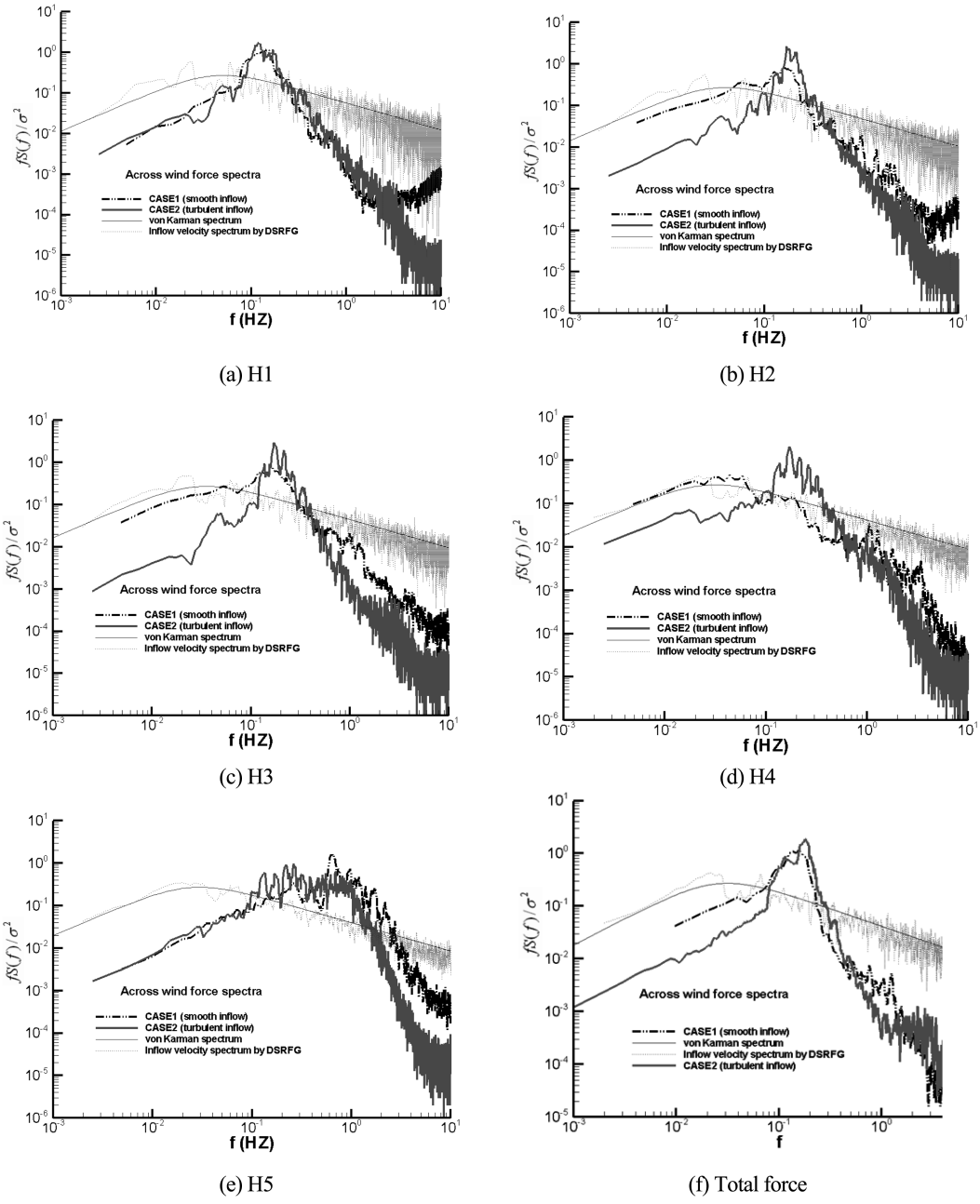

Fig. 13 Across-wind force spectra

frequency range is located in their main energy-containing subrange and low-frequency part of inertial subrange of power density. According to Lumley and Panofsky (1964)'s study, in a high Reynolds-number flow, the energy-containing subrange of turbulence contains the bulk of the turbulent energy and energy production source, and the inertial subrange contains the

Table 2 Turbulence length scales at five levels of inflow boundary

	Height (m)	U_{avg} (m/s)	L (m)	Local width (m)
H1	84 m~92.4 m	60	171	49.2
H2	168 m~176.4 m	66.3	239	48.6
H3	252 m~260.4 m	70.4	292	46
H4	336 m~344.4 m	73.4	336	48.6
H5	413 m~419.4 m	75.7	372	10

energy transferred from large scales of the energy containing range to smaller scales of the dissipation range. Therefore, it can be concluded that the energy contained in the inflow turbulence is rightly imposed in approaching flow and plays a right role in generation of the wind forces on the building surfaces for CASE2. Similar patterns are observed from Figs. 12(b)-12(e), as well as in Fig. 12(f) which show the total along-wind force spectra.

(2) Fig. 12(f) shows that for CASE2 the power density in frequency range of 0.4 HZ~1.5 HZ is relatively lower as compared with that for CASE1, while it has a local peak in frequency band near 2 HZ. It is noted that the frequency range from 0.4 HZ~1.5 HZ is mainly located in the inertial subrange of inflow turbulence, it seems that this part of inflow turbulence energy does not make a positive contribution to the resulted wind force. A reasonable explanation for such a phenomenon is that: the turbulent eddies in the main energy-containing subrange and part of the inertial subrange of inflow turbulence enhance their coupled frequency band of the vortex shedding (about 0.05~0.4 Hz) and thus the vortex movement in this frequency range is intensified, which leads to the increase of the force energy power density as discussed previously. With the intensification of vortex movement, the process of large scale vortices breaking up into small scale vortices is accelerated, which can be confirmed by the flow pattern comparison as shown in Fig. 7. Therefore, contribution of relative small scale vortices to the wind-induced force will be increased, which explains the local peak power density in frequency band near 2 Hz for CASE2.

(3) For the across-wind force F_L, the spectra of CASE2 present a typical sharp peak distribution, while those of CASE1 show a relatively smooth peak distribution. Similar with the situation observed from the along-wind force spectra, a decrease of spectral power density in frequency range 0.4 HZ~1.5 HZ is also observed for the spectra of CASE2 as compared with those of CASE1. It is believed to be caused by the same reason for the along-wind force discussed previously. It is noted that Fig. 13(e) presents a relative different pattern as those shown in other figures. It seems that there are two peaks, one is about at 0.15 Hz and the other is about at 0.9 Hz. This is because H5 is located on the tower atop the main building. The tower is subject to two streams of flow: one is the incoming flow and the other is the flow separated from the top edge of the main building. Obviously, the first induces a vortex shedding with a frequency about 0.15 Hz which can be estimated by Strouhal number (about 0.12 for a square cylinder); the latter itself is a separation flow with main frequency about 0.9 Hz. The coupling of these two streams of flow makes the resulted force spectra as shown in Figs. 12(e), 13(e) and 14(e).

(4) For the torsional moment M, the spectra of both the cases present a typical dual-peak distribution, although the sharpness of the second peak appears relatively flat. Compared with CASE1, the first peak of the power density for CASE2 is obviously attained to a higher value

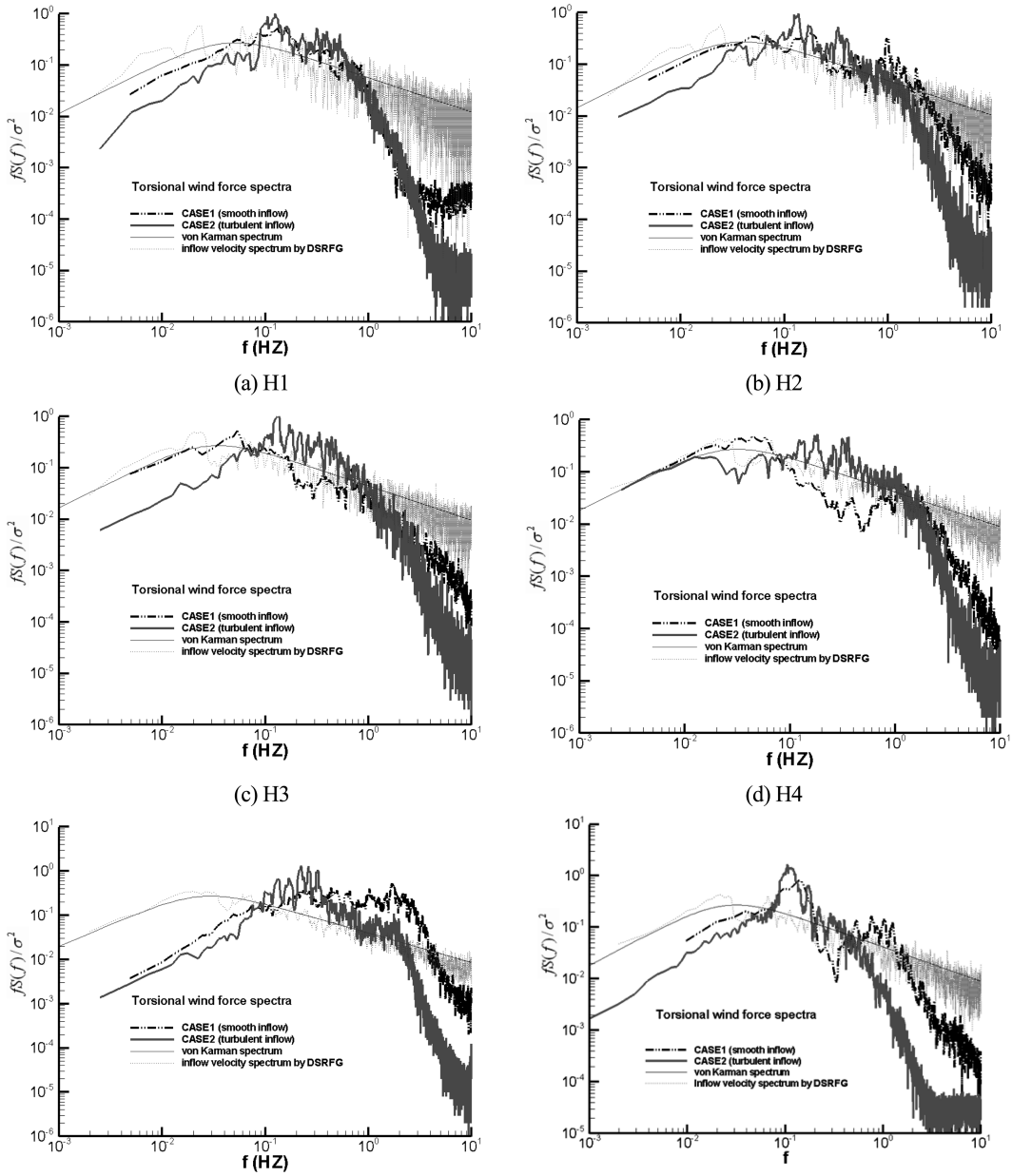

(a) H1 (b) H2

(c) H3 (d) H4

(e) H5 (f) Total force

Fig. 14 Torsional moment spectra

and they are all located in a frequency band between 0.1 Hz~0.2 Hz, which is corresponding to the peak power density range of the across-wind forces. For the second peak of power density, the corresponding frequency range is about 0.3 Hz~0.4 Hz for CASE2 while for CASE1 it is near 1 Hz, this discrepancy may be caused by the intensified along-wind force at the frequency band of 0.05 Hz~0.4 Hz for CASE2 as discussed previously.

Generally speaking, the effects of inflow turbulence on the wind forces on the super-tall building are significant and thus it is important to properly simulate the inflow field such as that for CASE2. From the detailed numerical study, the effects of strong winds on the World's tallest building are summarized as: Large turbulent eddies contained in approaching flows blow to Taipei 101 Tower, the fluctuations induced by these turbulent eddies are coupled with the lateral separation boundary layer, then the swaying of the lateral separation boundary layer is intensified by some kinds of resonance effects when the main frequency band of vortex shedding is coupled with the input fluctuations. The across-wind force is firstly intensified by such coupling effects when large scale vortices shed from the separation boundary layer near the building. A large number of vortices are quickly moving into the wake region, which induce a large pressure gradient on the back face of the building, and hence the dynamic component of the along-wind force is also intensified. The unsteady movements of vortices in the lateral and wake regions of the building also make the instantaneous pressure distributions on the building surfaces uneven and thus the torsional moment of the building is intensified. This is the mechanism to cause the wind-induced forces on the super-tall building.

4. Conclusions

The wind effects on 508 m high Taipei 101 Tower, under strong wind conditions were evaluated by LES with newly developed inflow turbulence generator and SGS model. The inflow turbulence generator was proved to be able to produce a fluctuating velocity flow field satisfying a target spectrum such the von Karman spectrum and prescribed profiles of turbulence intensity and integral length scale. The new SGS model is a combined model of the dynamic one-equation SGS model (Kajishima and Nomachi 2006) and the wall-adapting local eddy viscosity model (Nicoud and Ducros 1999), and was found to be suitable for relative coarse grid situations and simulation of high Reynolds number flows.

The present simulations were conducted with Reynolds number of about 1.8×10^8 based on the approaching wind speed at 10 m height and base width of Taipei 101 Tower. Totally two cases with and without generating inflow turbulence were taken into account in this study. Successful attempts were made to carry out LES with high Reynolds number for a full-scale size super-tall building and to investigate the effectiveness and accuracy of the developed inflow turbulence generator and the proposed SGS model. It is concluded from this study that:

1) The mean and dynamic forces on the super-tall building predicted by the present LES based on the inflow field generated by the DSRFG were found to match the available wind tunnel test data well. As a comparison, the case without generating inflow turbulence failed to predict the dynamic forces, indicating that the inflow turbulence is of great importance and necessity in the accurate evaluation of the dynamic wind loads on the tall building.

2) The DSRFG can generate a large number of random vortex-like patterns in oncoming flow. Vortex shedding patterns behind the building were obviously intensified, leading to a more contracted mean separation region and higher rms velocity values in the wake region.

3) It was observed from the SGS viscosity ratio contours that the dynamic mechanism of the proposed SGS model behaves correctly. For the present grid resolution, the SGS viscosity ratio is in the order of 500-6000.

4) Simulated force spectra revealed clear evidences of inflow turbulence's effects on the wind

force spectra. Detailed analysis showed that the resonance coupling of inflow fluctuation with the main frequency band of vortex shedding is the important mechanism of the resulted wind force spectra.

Generally speaking, the present SGS model integrated with the DSRFG technique could provide satisfactory predictions of the wind loads on the full-scale super-tall building. It is encouraging to obtain the numerical results comparable with the wind-tunnel test estimations, thus verifying the accuracy of the numerical frameworks presented in this paper. The recommended SGS model and the inflow turbulence generation technique as well as the associated numerical treatments are expected to be useful in practice for evaluation of design wind loads on tall buildings.

Acknowledgements

The work described in this paper was fully supported by a grant from the Research Grants Council of Hong Kong Special Administrative Region, China (Project No: CityU 116906), a grant from City University of Hong Kong (Project No: 7002466) and a key grant from National Natural Foundation of China (Project No. 90815030).

References

Baker, C.J. (2007), "Wind engineering-past, present and future", *J. Wind Eng. Ind. Aerod.*, **95**, 843-870.

Chorin, A.J. (1968), "Numerical solution of navier-stokes equations", *Math. Comput.*, **22**, 745-762.

Davies, M.E., Quincey, V.G. and Tindall, S.J. (1980), "The near-wake of a tall building block in uniform and turbulent flows", *Proceedings of the 5th International Conference on Wind Engineering Fort Collins,* (Ed. J.E. Cermak), Colorado, USA, July.

Fluent Inc. (2003), *The user guide of Fluent 6.2*.

Ferziger, J.H. and Peric, M. (1996), *Computational Methods for Fluid Dynamics*, Springer-Verlag, Heidelberg.

Gallerano, F., Pasero, E. and Cannata, G. (2005), "A dynamic two-equation sub-grid scale model", *Continuum Mech. Therm.*, **17**(2), 101-123.

Germano, M., Piomelli, U., Moin, P. and Cabot, W.H. (1991), "A dynamic subgrid scale eddy viscosity model", *Phys. Fluids*, **3**, 1760-1765.

Ghosal, S., Lund, T.S., Moin, P. and Akselvoll, K. (1995), "A dynamic localization model for large-eddy simulation of turbulent flows", *J. Fluid Mech.*, **286**, 229-255.

Huang, S.H., Li, Q.S. and Xu, S.L. (2007), "Numerical evaluation of wind effects on a tall steel building by CFD", *J. Constr. Steel Res.*, **63**(5), 612-627.

Huang, S.H., Li, Q.S. and Wu, J.R. (2010), "A General inflow turbulence generator for large eddy simulation", *J. Wind Eng. Ind. Aerod.*, **98**(10-11), 600-617.

Huang, S.H. and Li, Q.S. (2010), "A new dynamic one-equation subgrid-scale model for large eddy simulations", *Int. J. Numer. Meth. Eng.*, **81**(7), 835-865.

Jiang, D., Jiang, W.M., Liu, H. and Sun, J. (2008), "Systematic influence of different building spacing, height and layout on mean wind and turbulent characteristics within and over urban building arrays", *Wind Struct.*, **11**(4), 275-289.

Kajishima, T. and Nomachi, T. (2006), "One-equation subgrid scale model using dynamic procedure for the energy production", *J. Appl. Mech.-T. ASME*, **73**(3), 368-373.

Kijewski-Correa, T.L. (2003), *Full-scale Measurements and System Identification: A Time–Frequency Perspective*, PhD Thesis, The University of Notre Dame.

Kim, W.W. and Menon, S. (1995), *A new dynamic one-equation subgrid-scale model for large eddy simulations*, AIAA Paper No. 95-0356.

Kim, W.W. and Menon, S. (1999), "An unsteady incompressible Navier-Stokes solver for large eddy simulation of turbulent flows", *Int. J. Numer. Meth. Fl.*, **31**(6), 983-1017.
Krajnovic, S. and Davidson, L. (2002), "A mixed one-equation subgrid model for large-eddy simulation", *Int. J. Heat Fluid Fl.*, **23**(4), 413-425.
Leonard, B.P. (1991), "The ultimate conservative difference scheme applied to unsteady one-dimensional advection", *Comput. Method. Appl. M.*, **88**, 17-74.
Li, C., Li, Q.S., Huang, S.H., Fu, J.Y. and Xiao, Y.Q. (2010), "Large eddy simulation of wind loads on a long-span spatial lattice roof", *Wind Struct.*, **13**(1), 57-82.
Li, Q.S. and Melbourne, W.H. (1995), "An experimental investigation of the effects of free-stream turbulence on streamwise surface pressures in separated and reattaching flows", *J. Wind Eng. Ind. Aerod.*, **54-55**, 313-323.
Li, Q.S. and Melbourne, W.H. (1999), "The effects of large scale turbulence on pressure fluctuations in separated and reattaching flows", *J. Wind Eng. Ind. Aerod.*, **83**, 159-169.
Li, Q.S., Fang, J.Q., Jeary, A.P. and Wong, C.K. (1998), "Full scale measurement of wind effects on tall buildings", *J. Wind Eng. Ind. Aerod.*, **74-76**, 741-750.
Li, Q.S., Fang, J.Q., Jeary, A.P., Wong, C.K. and Liu, D.K. (2000), "Evaluation of wind effects on a super tall building based on full-scale measurements", *Earthq. Eng. Struct. D.*, **29**, 1845-1862.
Li, Q.S., Xiao, Y.Q., Wong, C.K. and Jeary, A.P. (2003), "Field measurements of wind effects on the tallest building in Hong Kong", *Struct. Des. Tall Spec.*, **12**(1), 67-82.
Li, Q.S., Wu, J.R., Liang, S.G., Xiao, Y.Q. and Wong, C.K. (2004), "Full-scale measurements and numerical evaluation of wind-induced vibration of a 63-story reinforced concrete tall building", *Eng. Struct.*, **26**(12), 1779-1794.
Li, Q.S., Xiao, Y.Q. and Wong, C.K. (2005), "Full-scale monitoring of typhoon effects on super tall buildings", *J. Fluid. Struct.*, **20**, 697-717.
Li, Q.S., Xiao, Y.Q., Wu, J.R., Fu, J.Y. and Li, Z.N. (2008), "Typhoon effects on super-tall buildings", *J. Sound Vib.*, **313**, 581-602.
Lilly, D.K. (1992), "A proposed modification of the Germano-subgrid-scale closure method", *Phys. Fluids*, **4**, 633-635.
Lumley, J.L. and Panofsky, H.A. (1964), *The structure of atmospheric turbulence*, Wiley-Interscience, New York.
Martinuzzi, R. (1992), *Experimentelle untersuchung der umstramung wandgebundener, rechteckiger, prismatischer Hindernisse*, Dissertation, University Erlangen-Nfirnberg.
Murakami, S. (1998), "Overview of turbulence models applied in CWE-1997", *J. Wind Eng. Ind. Aerod.*, **74-76**, 1-24.
Nicoud, F. and Ducros, F. (1999), "Subgrid-scale stress modelling based on the square of the velocity gradient tensor, *Flow Turbul. Combust.*, **62**, 183-200.
Nozu, T., Tamura, T., Okuda, Y. and Sanada, S. (2008), "LES of the flow and building wall pressures in center of Tokyo", *J. Wind Eng. Ind. Aerod.*, **96**, 1762-1773.
Nozawa, K. and Tamura, T. (2005), "Large eddy simulation of wind flows over large roughness elements", *Proceedings of the 4th European and African Conference on Wind Engineering (EACWE4)*, Prague, Cezch Republic.
Okamoto, M. and Shima, N. (1999), "Investigation for the one-equation-type subgrid model with eddy-viscosity expression including the shear-damping effect", *JSME Int. J. B-Fluid. T.*, **42**(2), 154-161.
Rodi, W. (1997), "Comparison of LES and RANS calculations of the flow around bluff bodies", *J. Wind Eng. Ind. Aerod.*, **71**, 55-75.
RWDI (1999), *Wind-induced structural responses cladding wind load study*, Roman Williams Davies and Irwin Inc.
Shiau, B.S. (2000), "Velocity spectra and turbulence statistics at the northeastern coast of Taiwan under high-wind conditions", *J. Wind Eng. Ind. Aerod.*, **88**(2-3), 139-151.
Smagorinsky, J. (1963), "General circulation experiments with the primitive equations. I. the basic experiment", *Mon. Weather Rev.*, **91**, 99-164.
Stathopoulos, T. (1997), "Computational wind engineering: Past achievements and future challenges", *J. Wind Eng. Ind. Aerod.*, **67-68**, 509-532.
Squires, K.D., Krishnan, V. and Forsythe, J.R. (2008), "Prediction of the flow over a circular cylinder at high

Reynolds number using detached-eddy simulation", *J. Wind Eng. Ind. Aerod*., **96**(10-11), 1528-1536.
Tamura, T. (2008), "Towards practical use of LES in wind engineering", *J. Wind Eng. Ind. Aerod*., **96**(10-11), 1451-1471.
Van Doormaal, J.P. and Raithby, G.D. (1984), "Enhancements of the SIMPLE method for predicting incompressible fluid flows", *Numer. Heat Tr. A-Appl*., **7**, 147-163.
Vreman, B., Geurts, B. and Kuerten, H. (1994), "On the formulation of the dynamic mixed subgrid-scale model", *Phys. Fluids*, **6**(12), 4057-4059.
Yoshizawa, A. and Horiuti, K. (1985), "A statistically-derived subgrid-scale kinetic energy model for the large-eddy simulation of turbulent flows", *J. Phys. Soc. Jpn*., **54**, 2834-2839.
Zang, Y., Street, R.L. and Koseff, J.R. (1993), "A dynamic mixed subgrid-scale model and its application to turbulent recirculating flows", *Phys. Fluids*, **5**(12), 3186-3196.
Zhang, N., Jiang, W.M. and Miao, S.G. (2006), "A large eddy simulation on the effect of buildings on urban flows", *Wind Struct*., **9**(1), 23-35.

CC